High-Sensitivity Raman Scattering Substrate Based on Au/$La_{0.7}Sr_{0.3}MnO_3$ Periodic Arrays

Ming-Chung Wu,[†] Yi Chou,[†] Chih-Min Chuang,[‡] Che-Pu Hsu,[§] Jhih-Fong Lin,[†] Yang-Fang Chen,*[,||] and Wei-Fang Su*[,†]

Department of Materials Science and Engineering, National Taiwan University, Taipei 106-17, Taiwan, Institute of Nuclear Energy Research, Atomic Energy Council (AEC), Taoyuan 325-46, Taiwan, Department of Chemical Engineering, National Taiwan University, Taipei 106-17, Taiwan, and Department of Physics, National Taiwan University, Taipei 106-17, Taiwan

ABSTRACT We have developed Au/$La_{0.7}Sr_{0.3}MnO_3$ (Au/LSMO) periodic arrays with tunable surface plasmon properties that can be used as novel surface-enhanced Raman scattering (SERS) substrates. The periodic arrays are created by electron beam lithography of LSMO resist and metal film deposition. The LSMO electron beam resist is unique in that it exhibits either positive or negative resist behaviors depending on the electron beam dosage. Interestingly, surface plasmon behavior of the arrays can be controlled by just changing the electron beam dosage when presented with a fixed design pattern. Scanning confocal microscopy and spectral microreflectometry have been adapted to directly demonstrate this unique behavior. Furthermore, we show that our novel Au/LSMO array can be used as a high-sensitivity Raman scattering substrate. To illustrate this working principle, the Au/LSMO periodic array is applied to enhance the Raman scattering of a thin film containing 0.1 wt % poly-3-hexylthiophene (P3HT) in poly(methyl methacrylate) (PMMA). By controlling the geometry of the patterned substrate that exhibits gold surface plasmon near the excitation wavelength, we can enhance the intensity of Raman scattering of P3HT at 1350 cm^{-1} up to 4 orders of magnitude as compared with previously generated planar Au substrates.

KEYWORDS: surface plasmon • $La_{0.7}Sr_{0.3}MnO_3$ • poly-3-hexylthiophene • surface-enhanced Raman scattering • Raman mapping

INTRODUCTION

Over the past decade, interest in the fabrication of periodic metallic structures has rapidly increased due to its surface plasmon resonance (SPR) behavior (1, 2). Coupling a radiation dipole with a surface plasmon generated on the surface of noble metals can lead to effective energy transfer from the dipole into the SPR. SPR is strongly dependent on the size (3, 4), shape (5−8), surface state (9), surrounding environment (10), metal features (11), and metal thickness (12). The metallic interfaces also play complex roles in the basic interactions of an electromagnetic field with optically active materials. Gold and silver are the most widely used metals for the surface plasmon resonance research (13−15). Many approaches have been established to investigate SPR, such as colloidal lithography (16, 17), electron beam lithography (18, 19), block copolymers with incorporated nanoparticles (20, 21), self-assembled monolayers (9, 22), reversal imprinting-in-metal process (23), photolithography (14), etc. Moreover, SPR behavior has been utilized in making organic plasmon-emitting diodes (24, 25), waveguides (1), Bragg reflectors (1, 26−28), resonators (29), biochemical sensors (30), and surface-enhanced Raman scattering substrates (2, 31, 32).

Previous SPR studies have focused on producing an ever larger effect of surface-enhanced Raman scattering (SERS) by varying the geometry of the metallic structures (11, 33). The increased intensity of Raman scattering from vibrational bands of a molecule at a metal's nanoparticle surface can be achieved by using the extremely high local electromagnetic fields of molecules associated with local surface plasmon resonance (18, 34, 35). Rough metallic surfaces can enhance the radiation from nearby organic dyes through nonradiative energy transfer, while the molecules adsorbed onto metallic electrodes show several orders of magnitude increase in SERS (36). Gold nanohole arrays are excellent candidates for use as SERS substrates because of the light confinement effects that happen between the nanohole arrays, which provide large tolerance dimensions and empty space as confined by the nanoholes. A strong SERS effect on gold nanohole arrays has been observed for 4-mecaptopyridine (18, 37). Käll et al. also fabricated some substrates for surface Raman scattering that exhibit a controlled electrocoupling between Ag nanoparticles (32). Tsukruk et al. demonstrated a 3D porous nanocanal array decorated with gold nanoparticles that can achieve 5 orders of Raman enhancement of 2,4-dinitrotoluene as compared with a conventional planar nanoparticle array (38). Nie et al. observed a large Raman scattering enhancement in vivo for tumor detection (30). All the above examples involve time-consuming multistep processes to obtain a surface plasmon resonance substrate that has an optimal enhanced Raman scattering effect.

[†] Department of Materials Science and Engineering, National Taiwan University.
[‡] Institute of Nuclear Energy Research, Atomic Energy Council (AEC).
[§] Department of Chemical Engineering, National Taiwan University.
[||] Department of Physics, National Taiwan University.
Received for review June 29, 2009 and accepted October 4, 2009
DOI: 10.1021/am900445e

Published on Web 10/28/2009

Periodic arrays with tunable optical properties have been fabricated by an electron beam $La_{0.7}Sr_{0.3}MnO_3$ (LSMO) zwitter resist using a single fixed design electron beam pattern without changing the geometries and lattice constants of the periodical structures. These arrays were fabricated by simply changing the electron beam dosage (39, 40). This technique provides a convenient and direct fabrication process for optoelectronic devices. Moreover, the periodic patterns made of LSMO zwitter resist exhibit good chemical stability as compared with conventional polymer zwitter resist. This is because the pattern is made of an inert metal oxide and it shows a good chemical stability for most of the organic solvent. In this study, we use an LSMO resist to easily generate SERS substrates with tunable surface plasmon behaviors. These substrates enhanced the Raman scattering signal by 4 orders of magnitude as films consisting of low-concentration (0.1 wt %) P3HT in PMMA. Therefore, this new patterned Au/LSMO composite is an excellent improvement over current technology and serves as a template for the future development of many other optoelectronic devices and biosensors.

EXPERIMENTAL SECTION

The LSMO electron beam resist was prepared by dissolving 8.58 wt % of lanthanum nitrate ($La(NO_3)_3 \cdot 6H_2O$, Acros, 98%), strontium nitrates ($Sr(NO_3)_2$, Fluka, 98%), manganese nitrates ($Mn(NO_3)_2 \cdot 4H_2O$, Fluka, 97%), and 1.75 wt % polyvinyl alcohol (PVA, Acros, 88%, 22 000 g/mol) in water with the molar ratio La:Sr:M_n = 0.7:0.3:1.0. The precursor solution was stirred for 48 h at 50 °C. After the precursor solution was filtered through syringe filters (0.22 μm), the precursor solution was spin-coated at 1000 rpm for 90 s to give a nominal thickness of about 200 nm. The thickness of the water-developable LSMO resist-coated on a silicon wafer was measured directly by an alpha-stepper (Veeco, Tektak3). High-resolution nanolithography was performed by using a Hitachi ELS-7500EX machine to write the specific patterns across a 150 × 150 μm field with a 2.5 nm beam step size. The electron beam writer system was operated at 50 kV with a probe current of 1.0 nA. A sample containing a 2 × 5 and 2 × 4 array field was irradiated with a starting dose time of 0.1 μs and then with additional dose increments of 0.1 and 1.0 μs per field. Deionized water was used to develop the LSMO resist at 50 °C for 30 s. These patterned LSMO structures on a silicon wafer were then deposited on a 20 nm thick gold film by using a thermal evaporator (ULVAC) to make Au/LSMO arrays. This process produced Au/LSMO arrays that averaged 40 × 40 μm^2.

Field-emission scanning electron microscopy (FE-SEM, Elionix, ERA-8800FE, Japan) was used to observe the microstructures of the Au/LSMO arrays, and atomic force microscopy (AFM, Digital Instruments, Dimension-3100 Multimode) was used to measure the surface topography of the Au/LSMO periodic arrays. The extinction spectra of Au/LSMO samples were evaluated using a spectral microreflectometer (Mission Peak Optics, MP100-ME) equipped with an optical microscope. Unpolarized light was focused on the composite film under the silicon substrate at a spot size <20 μm to measure the interference between the incident and reflected light with wavelengths ranging from ultraviolet to near-infrared (250−1000 nm). To measure the extinction spectra of Au/LSMO periodic arrays, it is necessary to first measure the ambient environmental light with the light source off. Next, the nonpatterned area of the sample is placed on the stage and brought into focus to measure the reflected signals from the wavelength of 250−1000 nm. These measurements are considered background reflected signal. Finally, the reflected light signals of Au/LSMO periodic arrays are measured from 250 to 1000 nm. The loss signals from 250 to 1000 nm can be calculated by using the Mission Peak Optics program. This yields the final extinction spectrum measurement of the Au/LSMO sample from wavelengths of 250 to 1000 nm.

The extinction behavior maps of the patterned Au-coated LSMO samples were measured by scanning confocal microscopy (WITec, AlphaSNOM, Germany). The scanning images were collected using a high-resolution piezoelectric stage (PI). Three kinds of excitation lasers, argon ion laser (λ_{exc} 488 nm), Nd:YAG laser (λ_{exc} 532 nm), and He−Ne laser (λ_{exc} 632.8 nm), with different output powers, were employed as radiation sources. The reflected light was collected with a 100X Nikon plane objective (NA ≈ 0.9) and detected with a single photon counting photomultiplier tube (PMT). For each line scan, 512 data points were taken with a line scan frequency of 0.5 Hz.

To prove the SERS effect of our Au/LSMO substrate, we used a model matter made from a film consisting of the polymer blend of 0.1 wt % of P3HT in PMMA. The film was obtained by spin-coating a solution on the SERS substrate. The solution is made from 0.2 wt % of polymer blend in chlorobenzene. P3HT with low molecular weight (8.1 kDa) and high regiospecificity (>95%) was synthesized according to the literature with some modifications (41). 2,5-Dibromo-3-hexylthiophene (0.030 mol, 10.000 g) was added into a 500.0 mL three-neck round-bottom flask equipped with a 24/40 ground joint, a reflux condenser, and a magnetic stir bar. It was purged with dry nitrogen for 15 min. A 320.0 mL portion of freshly distilled tetrahydrofuran (THF) was transferred to the flask, and the solution was stirred under dry nitrogen. A solution of *tert*-butylmagnesium chloride in diethyl ether (0.032 mol, 16.0 mL) was added via an airtight syringe and then kept at room temperature for 0.5 h. The solution was cooled to room temperature, followed by the addition of $Ni(dppp)Cl_2$ (2 mol % of monomer, 0.332 g) and stirring at room temperature for 0.5 h. This solution was poured into methanol (500.0 mL). This action led to precipitation, and the solid was collected in a cellulose extraction thimble and then washed with methanol in a Soxhlet apparatus. The polymer was dried under vacuum overnight and gathered as a dark purple material (60% yield). The MWs and polydispersity (PDI) values of P3HT were determined by gel permeation chromatography (GPC) on a Waters 1525 Binary HPLC Pump with polystyrene as standard and tetrahydrofuran (THF) as the solvent. The regiospecificity (RR) of P3HT was determined by NMR spectroscopy using a Bruker AVANCE 400 spectrometer with $CDCl_3$ as solvent and tetramethylsilane as an internal standard. A mixture of 0.001 g of P3HT and 0.999 g of poly(methyl methacrylate) (PMMA, MW ≈ 996k, Aldrich) in 49.000 g of chlorobenzene was stirred for 48 h to obtain a polymer solution. Then, the solution was spin-coated on the Au/LSMO substrate. Finally, we could obtain a P3HT/PMMA film coated on patterned Au/LSMO substrate with different geometries, including hole arrays and disk arrays. Scheme 1 illustrates the fabrication process.

Scanning confocal Raman mapping measurements were conducted with a confocal microscope (WITec, CMR200, Germany) in the backscattering mode. A diffraction-limited confocal Raman microscope gives a lateral spatial resolution (~300 nm) about half of the excitation wavelength (λ_{exe} 632.8 nm). The Raman image mapping was obtained by intensity integration of the spectra by recording the data with 450 nm/step and an integration time of 1 s/step. In all cases, the laser beam was focused down with a 100X, with numerical aperture = 0.95 objective (Olympus), and the focused laser beam was about 1.0 μm in diameter, corresponding to about 2−3 pixels in the integrated Raman image.

Scheme 1. Schematic Illustration of the Fabricating Process of P3HT/PMMA Film Coated on Patterned Au/LSMO Substrate: (a) Coat LSMO Resist on Silicon; (b) Create LSMO Pattern by Electron Beam Lithography; (c) Evaporate Au Thin Film on the LSMO Pattern; (d) Coat P3HT/PMMA Film on Au/LSMO Pattern

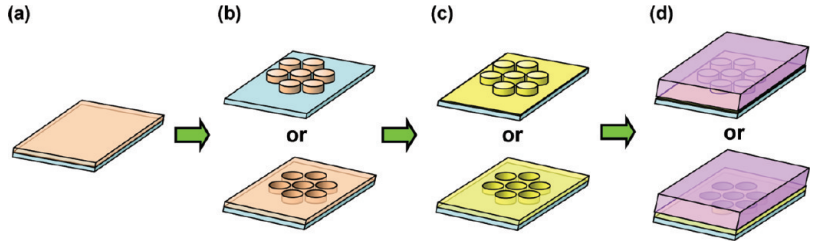

RESULTS AND DISCUSSION

The LSMO resist shows both positive and negative characteristics when varying electron dosage, and this particular feature then can be used to adjust the surface topography when using one fixed design pattern (42). In this study, we have used a LSMO zwitter resist to fabricate Au/LSMO periodic arrays with modulated surface plasmon resonance phenomena. We were able to fabricate a high-quality continuous gold film with a thickness of 20 nm. Figure 1 shows a clear SEM image of a 20 nm Au coated LSMO sample. Therefore, 20 nm Au was selected as the optimal thickness for preparation of all the samples used in this research. The Au-coated LSMO hole array and the disk array were obtained using medium electron dosage (19.2 mC/cm^2) and high electron dosage (192.0 mC/cm^2), respectively. Here, a fixed design pattern of 300 nm in diameter and 500 nm in lattice constant was employed.

For a confined geometry, the surface plasmon is generally localized and its resonance frequency depends on the size and shape of the metallic material. The extinction spectra can be modulated either by changing the radius with a fixed lattice constant or by changing the lattice constant with a fixed radius. For the hole structure, we have studied the extinction spectra of the Au/LSMO periodic array with a fixed hole diameter of 300 nm and different lattice constants of 500, 700, and 900 nm, and the results are shown in Figure 2a. All the samples were prepared using a medium dosage of the electron beam (16.0 mC/cm^2), so that their refractive indexes (samples A−C) are similar, and the value is around 2.05 measured by prism coupler (2010/M, Metricon). Each extinction curve of the samples was obtained by a spectral microreflectometer equipped with an optical microscope. The extinction spectra of Au/LSMO periodic hole arrays show a blue shift of λ_{max} from 483 nm to 471 nm and then to 453 nm with an increase in the lattice constant of periodic hole arrays from 500 nm to 700 nm and to 900 nm, respectively. Moreover, for Au/LSMO periodic disk arrays, the extinction spectra of the arrays show a blue shift from 492 nm to 460 nm and then to 445 nm when the arrays are obtained from a fixed 300 nm disk diameter and different lattice constants: 500, 700, and 900 nm (Figure 2b; samples D−F, respectively). Thus, the extinction spectra of both periodic Au/

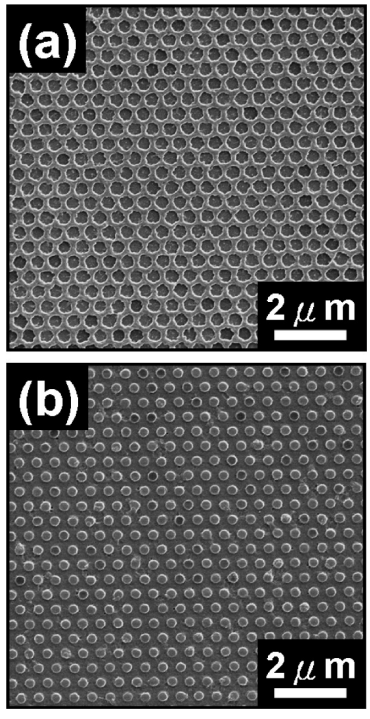

FIGURE 1. SEM images of Au-coated LSMO periodic array: (a) periodic hole array; (b) periodic disk array.

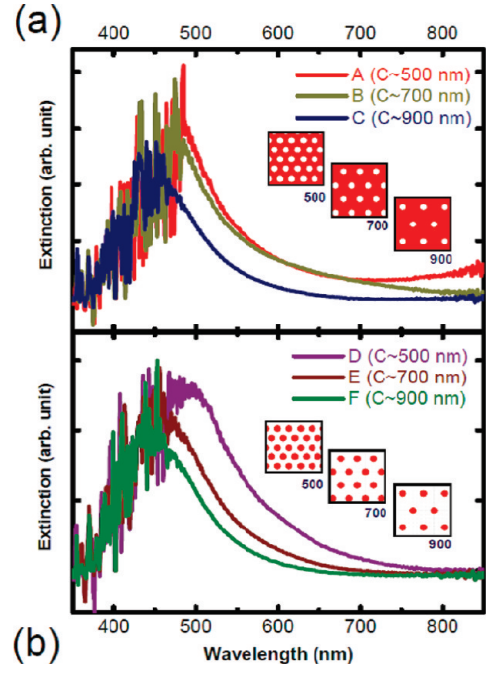

FIGURE 2. Extinction spectra of Au/LSMO periodic arrays with different geometries: (a) Au/LSMO periodic hole arrays with different lattice constants; (b) Au/LSMO periodic disk arrays with different lattice constants.

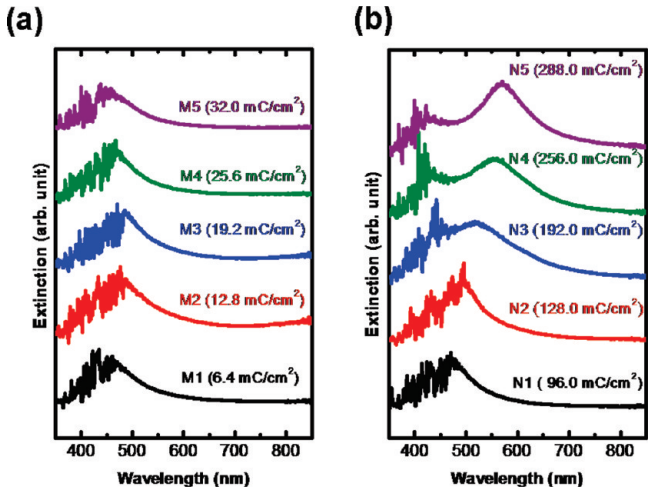

FIGURE 3. Extinction spectra of Au/LSMO arrays fabricated with different electron dosages using a fixed design of 300 nm diameter and 500 nm lattice constant. Each curve represents a sample obtained at specific electron irradiation, as indicated above the curve: (a) periodic Au/LSMO hole arrays; (b) periodic Au/LSMO disk arrays.

LSMO disk arrays exhibit blue shifts and decrease in intensity when the lattice constant is increased. Furthermore, the periodic Au/LSMO hole arrays exhibit a surface plasmon resonance that is qualitatively similar to the surface plasmon of the periodic disk arrays.

The extinction spectrum of Au/LSMO periodic arrays can also be controlled using a designed pattern of fixed column diameter and lattice constant by varying the electron beam dosage. At medium electron doses (6.4−32.0 mC/cm^2), the LSMO resist generates positive patterns. The spectrum of the arrays is red-shifted from 443 to 486 nm (M1−M3) after increasing the electron beam dosage from 6.4 mC/cm^2 to 19.2 mC/cm^2 but is blue-shifted from 486 to 457 nm (M3−M5) on further increasing the dosage to 32.0 mC/cm^2, as shown in Figure 3a. The results are due to the changing of Au/LSMO periodic hole arrays in the z direction. The hole depth varies from 31.89 to 34.64 nm (M1−M3) for the positive behavior of the resist and then returns to 31.46 nm (M3−M5) for the negative behavior of the resist. For the Au/LSMO periodic disk arrays, we can observe the λ_{max} of the extinction peaks shows an obvious red shift from 469 to 571 nm (curve N1 to curve N5, Figure 3b). These behaviors result from the increasing z dimension of disk arrays. The height of the LSMO disk arrays is increased from 34.04 nm (N1) to 80.76 nm (N5) with an increase in the exposed electron dosage from 96.0 to 288.0 mC/cm^2. We have adapted the empirical equation of El-Sayed et al. (43) derived from universal scaling behavior to predict the wavelength shift as shown:

$$\frac{\Delta\lambda}{\lambda_0} \approx A \exp\left(-\frac{s/D}{B \cdot H}\right) \quad (1)$$

where $\Delta\lambda/\lambda_0$ is the fractional plasmon shift, s is the lattice constant, D is the diameter of hole or disk, A and B are the coefficients, and H is the hole depth or disk height. The amount of wavelength shift calculated from eq 1 is consistent with the experimental results, which reveal that the LSMO resist can be used to modulate gold surface plasmon resonance by varying the z dimension of the LSMO with a fixed design pattern.

We have used a scanning confocal microscope equipped with different excitation lasers (488, 532, and 632.8 nm) to directly observe the difference of extinction properties between the patterned area and nonpatterned area. The differences can be expressed using the equation

$$\mathrm{EF} = \frac{E_0 - E_p}{E_0} \quad (2)$$

where EF is the extinction factor, E_0 is the average photon count of the nonpatterned area, and E_p is the average photon count of the patterned area. The extinction behaviors of the M3 hole pattern (Figure 4a−c) and N3 disk pattern (Figure 4d−f) were studied and analyzed. A high contrast in extinction behavior mapping represents a high extinction factor. The EF of M3 is decreased from 0.711 (Figure 4a) to 0.584 (Figure 4b) and then to 0.478 (Figure 4c) with increasing excitation wavelength from 488 nm to 532 nm and then to 632.8 nm, respectively. This result is expected, since the extinction peak λ_{max} of the M3 sample (486 nm) is close to the 488 nm excitation wavelength. For the λ_{max} of the N3 sample at 520 nm, an increased EF from 0.680 (Figure 4d) to 0.688 (Figure 4e) is expected, when the excitation wavelength is increased from 488 nm to 532 nm. A decreased EF from 0.688 (Figure 4e) to 0.347 (Figure 4f) was observed, which results from the increasing excitation wavelength from 532 to 632.8 nm.

In order to confirm the effect of surface-enhanced Raman scattering on our Au/LSMO SERS substrate, we used a model matter made from 0.1 wt % P3HT in PMMA to coat on the Au/LSMO SERS substrate. By intensity integration of the spectral domain ranging from 600 to 2900 cm^{-1}, we can observe the contrast of P3HT Raman scattering signals between patterned and nonpatterned areas on an Au-coated LSMO hole array, as shown in Figure 5. Sample M3 has the highest Raman scattering contrast when compared with other samples, due to the fact that the surface plasmon resonance of M3 is closer to the excitation wavelength of the He−Ne laser.

For the Au/LSMO periodic disk arrays (N series samples), N5 gives the strongest Raman scattering signals among the N series samples (Figure 6), because the λ_{max} (571 nm) of N5 is the closest to the excitation wavelength of 632.8 nm. Thus, as the peak position of surface plasmon resonances approaches the excitation laser wavelength of 632.8 nm, we are able to obtain a larger enhancement of the Raman scattering of P3HT/PMMA. The enhancement in Raman scattering signals mainly results from an efficient energy transfer from gold surface plasmon to the P3HT/PMMA film. Moreover, we have measured the exact enhancement factor from the Raman spectra of P3HT/PMMA film on Au/LSMO substrate, as shown in Figure 7. Because the enhancement

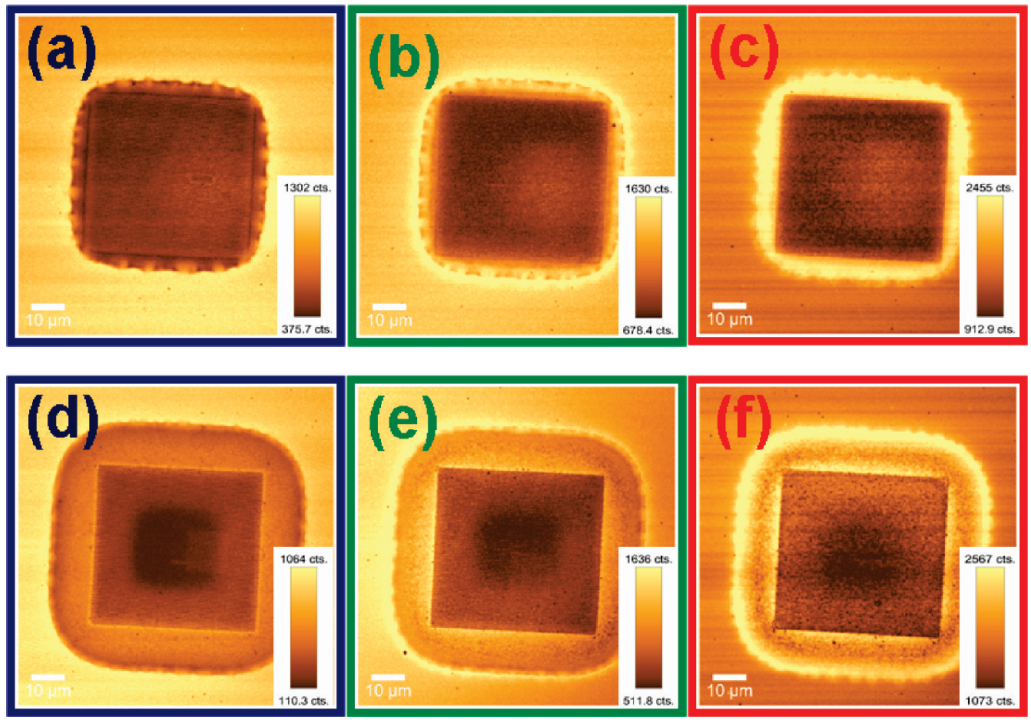

FIGURE 4. Extinction behavior mapping of the Au/LSMO periodic hole array, with samples of M3 (a–c), and of the Au/LSMO periodic disk array, with samples of N3 (d–f), excited by different excitation lasers: (a, d) samples excited by 488 nm Ar ion laser; (b, e) samples excited by 532 nm Nd:YAG laser; (c, f) samples excited by 632.8 nm He–Ne laser.

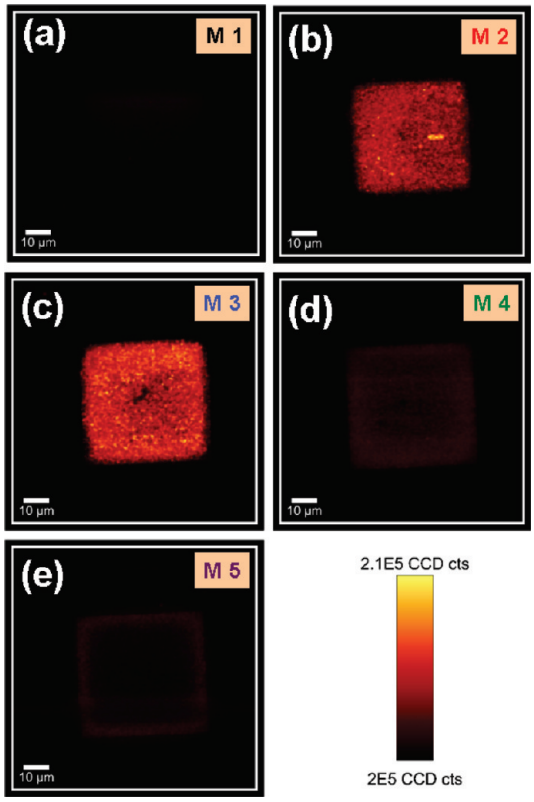

FIGURE 5. Raman mapping images of P3HT/PMMA coated on the Au/LSMO SERS substrate fabricated by medium electron dosage (6.4–32.0 mC/cm^2), with all samples excited by 632.8 nm He–Ne laser: (a) λ_{max} of M1 array 443 nm; (b) λ_{max} of M2 463 nm; (c) λ_{max} of M3 486 nm; (d) λ_{max} of M4 475 nm; (e) λ_{max} of M5 array 457 nm.

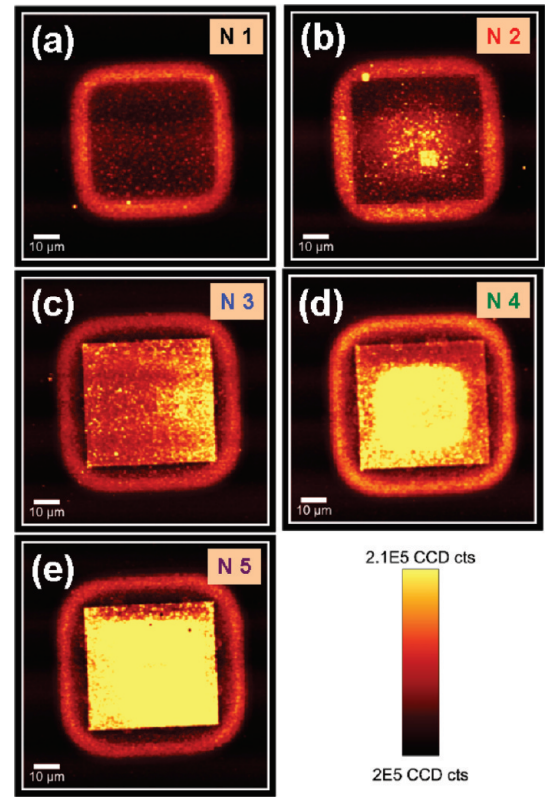

FIGURE 6. Raman mapping of P3HT/PMMA coating on the LSMO SERS substrate fabricated by high electron dosage (96.0–288.0 mC/cm^2), with all samples excited by 632.8 nm He–Ne laser: (a) λ_{max} of N1 array 469 nm; (b) λ_{max} of N2 array 495 nm; (c) λ_{max} of N3 array 518 nm; (d) λ_{max} of N4 array 555 nm; (e) λ_{max} of N5 array 571 nm.

is so large, we have to reduce the spectrum collective time of the patterned area to 1/10 (0.1 s) compared to that of the nonpatterned area (N-0). For the P3HT/PMMA film, the prominent Raman bands at 1547 and 1350 cm^{-1} result from

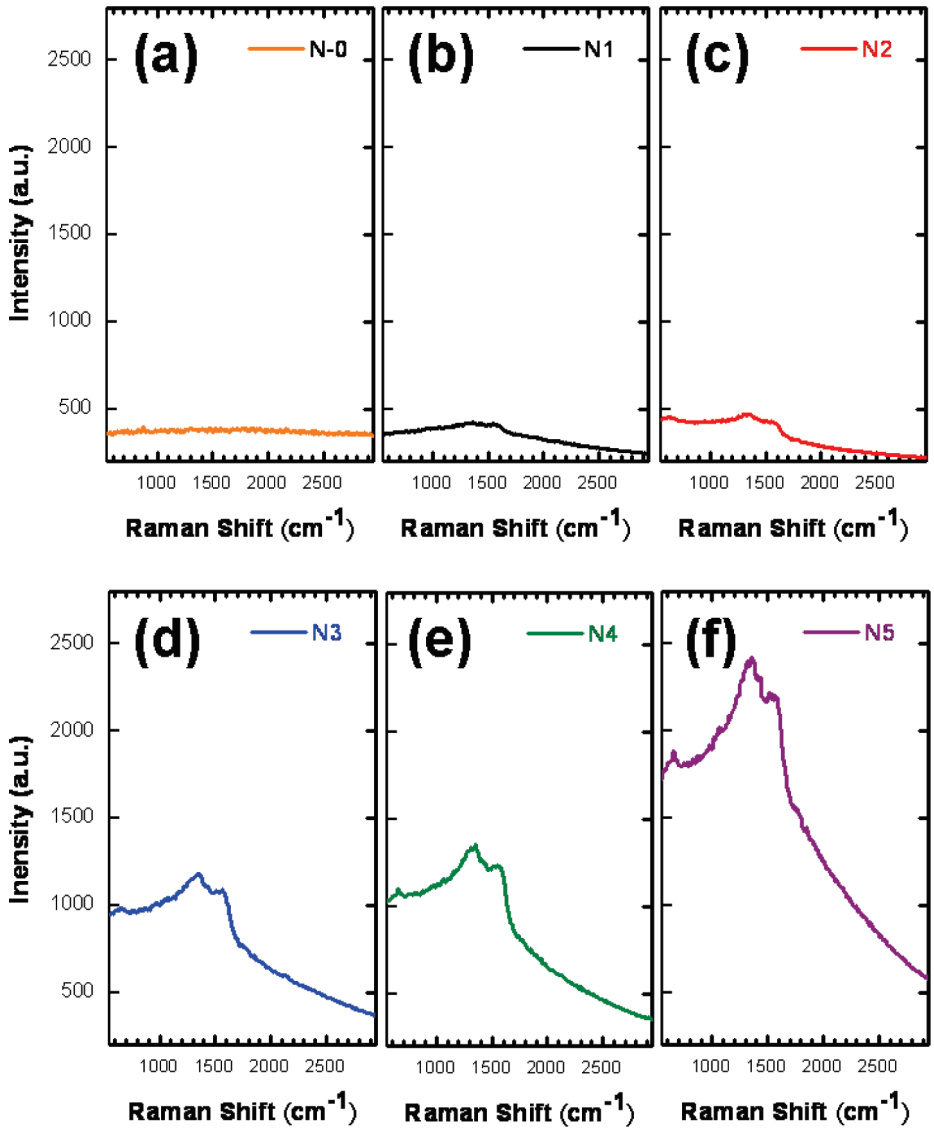

FIGURE 7. Raman spectra of P3HT/PMMA coating on the LSMO SERS substrate fabricated by high electron dosage (96.0−288.0 mC/cm^2), with all samples excited by 632.8 nm He−Ne laser: (a) N-0, nonpatterned area exhibiting no surface plasmon resonance; (b) λ_{max} of N1 array 469 nm; (c) λ_{max} of N2 array 495 nm; (d) λ_{max} of N3 array 518 nm; (e) λ_{max} of N4 array 555 nm; (f) λ_{max} of N5 array 571 nm.

the C═C stretching vibrations of the thiophene ring and C−C skeletal stretching, respectively. The peak at 661 cm^{-1} is assigned to the deformation vibration of the C−S−C bonds. The N5 sample shows the largest Raman scattering signal enhancement of up to 4 orders at 1350 cm^{-1}.

CONCLUSIONS

We have fabricated Au/LSMO periodic arrays with tunable surface plasmon properties, which are very useful to serve as novel surface-enhanced Raman scattering (SERS) substrates. By controlling the gold surface plasmon close to the excitation wavelength, we demonstrated that the Raman scattering signals of P3HT/PMMA film can be enhanced by up to 4 orders of magnitude. It is worth noting that the LSMO electron beam resist can exhibit both positive and negative resist behaviors depending on the electron beam dosage, which is quite unique and convenient for the manipulation of patterned structures. Therefore, this new patterned Au/LSMO composite is an excellent improvement over current technology and serves as a template for the future development of many other optoelectronic devices and sensors.

Acknowledgment. Financial support obtained from the National Science Council of Taiwan (Project No. NSC95-3114-P-002-003-MY3 and NSC96-2628-E-002-017-MY3) is highly appreciated. We also thank Prof. Chieh-Hsiung Kuan and Prof. Ruey-Lin Chern of National Taiwan University for helpful discussions, Mr. Wei-Che Yen, Mr. Yu-Chia Liao, and Ms. Sharon Chen of National Taiwan University for materials synthesis and fabrication process, and Mr. A. J. Su of Duquesne University (Pittsburgh, PA) for editing the manuscript. The electron beam lithography was carried out using the Elionix facility located in the Center for Information and Electronics Technologies of National Taiwan University.

Supporting Information Available: Text and a figure giving a description of the experimental method for measuring extinction spectra. This material is available free of charge via the Internet at http://pubs.acs.org.

REFERENCES AND NOTES

(1) Barnes, W. L.; Dereux, A.; Ebbesen, T. W. *Nature* **2003**, *424*, 824.
(2) Ko, H.; Singamaneni, S.; Tsukruk, V. V. *Small* **2008**, *4*, 1576.
(3) Xiong, Y.; Chen, J.; Wiley, B.; Xia, Y.; Yin, Y.; Li, Z. Y. *Nano Lett.* **2005**, *5*, 1237.
(4) Chern, R. L.; Liu, X. X.; Chang, C. C. *Phys. Rev. E* **2007**, *76*, 016609.
(5) Lu, L.; Kobayashi, A.; Tawa, K.; Ozaki, Y. *Chem. Mater.* **2006**, *18*, 4894.
(6) Lu, G.; Li, C.; Shi, G. *Chem. Mater.* **2007**, *19*, 3433.
(7) Wei, H.; Hao, F.; Huang, Y.; Wang, W.; Nordlander, P.; Xu, H. *Nano Lett.* **2008**, *8*, 2497.
(8) Chern, R. L.; Chang, C. C.; Chang, C. C. *Phys. Rev. E* **2006**, *73*, 036605.
(9) Chen, C. F.; Tzeng, S. D; Chen, H. Y.; Lin, K. J.; Gwo, S. *J. Am. Chem. Soc.* **2008**, *130*, 824.
(10) Prikulis, J.; Hanarp, P.; Olofsson, L.; Sutherland, D.; Käll, M. *Nano Lett.* **2004**, *4*, 1003.
(11) Okamoto, K.; Niki, I.; Shvartser, A.; Narukawa, Y.; Mukai, T.; Scherer, A. *Nat. Mater.* **2004**, *3*, 601.
(12) Park, T. H.; Mirin, N.; Lassiter, J. B.; Nehl, C. L.; Halas, N. J.; Nordlander, P. *ACS Nano* **2008**, *2*, 25.
(13) Chuang, C. M.; Wu, M. C.; Su, W. F.; Cheng, K. C; Chen, Y. F. *Appl. Phys. Lett.* **2006**, *89*, 061912.
(14) Tsai, M.W.; Chuang, T.H.; Chang, H.Y.; Lee, S.C. *Appl. Phys. Lett.* **2006**, *89*, 093102.
(15) Rindzevicius, T.; Alaverdyan, Y.; Sepulveda, B; Pakizeh, T.; Kall, M.; Hillenbrand, R.; Aizpurua, J.; Javier Garcia de Abajo, F. *J. Phys. Chem. C* **2007**, *111*, 1207.
(16) Yang, S.-M.; Jang, S. G.; Choi, D.-G.; Kim, S.; Yu, H. K. *Small* **2006**, *2*, 458.
(17) Chan, G. H.; Zhao, J.; Hicks, E. M.; Schatz, G. C.; Duyne, R. P. V. *Nano Lett.* **2007**, *7*, 1947.
(18) Yu, Q.; Guan, P.; Qin, D.; Golden, G.; Wallance, P. M. *Nano Lett.* **2008**, *8*, 1923.
(19) Wu, M. C.; Chuang, C. M.; Lo, H. H.; Cheng, K. C.; Chen, Y. F.; Su, W. F. *Thin Solid Films* **2008**, *517*, 863.
(20) Chiu, J. J.; Kim, B. J.; Kramer, E. J.; Pine, D. J. *J. Am. Chem. Soc* **2005**, *127*, 5036.
(21) Chiu, J. J.; Kim, B. J.; Yi, G. R.; Bang, J.; Kramer, E. J.; Pine, D. J. *Macromolecules* **2007**, *40*, 3361.
(22) Wei, A.; Kim, B.; Sadtler, B.; Tripp, S. L. *Chem. Phys. Chem.* **2001**, *21*, 743.
(23) Chen, H. L.; Chuang, S. Y.; Lee, W. H.; Kuo, S. S.; Su, W. F.; Ku, S. L.; Chou, Y. F. *Opt. Express* **2009**, *17*, 1636.
(24) Shen, K. C.; Chen, C. Y.; Chen, H. L.; Huang, C. F.; Kiang, Y. W.; Yang, C. C.; Yang, Y. J. *Appl. Phys. Lett.* **2008**, *93*, 231111.
(25) Koller, D. M.; Hohenau, A.; Ditlbacher, H.; Galler, N.; Reil, F.; Aussenegg, F. R.; Leitner, A.; List, E. J. W.; Krenn, J. R. *Nat. Photonics* **2008**, *2*, 684.
(26) Kottmann, J. P.; Martin, O. J. F.; Smith, D. R.; Schultz, S. *Phys. Rev. B* **2001**, *64*, 5402.
(27) Weeber, J. C.; Dereux, A.; Girard, C.; Krenn, J. R.; Goudonnet, J. P. *Phys. Rev. B* **1999**, *60*, 9061.
(28) Weeber, J. C.; Krenn, J. R.; Dereux, A.; Lamprecht, B.; Lacroute, Y.; Goudonnet, J. P. *Phys. Rev. B* **2001**, *64*, 045411.
(29) Dmitriev, A.; Pakizeh, T.; Käll, M.; Sutherland, D. S. *Small* **2007**, *3*, 294.
(30) Qian, X.; Peng, X. H.; Ansari, D. O.; Goen, Q. Y.; Chen, G. Z.; Shin, D. M.; Yang, L.; Young, A. N.; Wang, M. D.; Nie, S. *Nat. Biotechnol.* **2008**, *26*, 83.
(31) Haes, A. J.; Duyne, R. P. V. *J. Am. Chem. Soc.* **2002**, *124*, 10596.
(32) Gunnarsson, L.; Bjerneld, J.; Xu, H; Petronis, S.; Kasemo, B.; Käll, M. *Appl. Phys. Lett.* **2001**, *78*, 802.
(33) Song, J. H.; Atay, T.; Shi, S.; Urabe, H.; Nurmikko, A. V. *Nano Lett.* **2005**, *5*, 1557.
(34) Xu, H.; Käll, M. *Top. Appl. Phys.* **2006**, *103*, 87.
(35) Tian, Z. Q.; Ren, B.; Wu, D. Y. *J. Phys. Chem. B* **2002**, *106*, 9463.
(36) Johansson, P; Xu, H.; Käll, M. *Phys. Rev. B* **2005**, *72*, 035427.
(37) Wei, H.; Håkanson, U.; Yang, Z.; Höök, F.; Xu, H. *Small* **2008**, *4*, 1296.
(38) Ko, H.; Tsukruk, V. V. *Small* **2008**, *4*, 1980.
(39) Wu, M. C.; Chuang, C. M.; Chen, Y. F.; Su, W. F. *J. Mater. Chem.* **2008**, *18*, 780.
(40) Wu, M. C.; Chuang, C. M.; Lin, J. F.; Huang, Y. C. *J. Mater. Res.* **2009**, *24*, 394.
(41) Loewe, R. S.; Khersonsky, R. D.; McCullough, R. S. *Adv. Mater.* **1999**, *11*, 250.
(42) Chuang, C. M.; Wu, M. C.; Huang, Y. C.; Cheng, K. C.; Lin, C. F.; Chen, Y. F.; Su, Y. F. *Nanotechnology* **2006**, *17*, 4399.
(43) Jain, P. K.; Huang, W.; El-Sayed, M. A. *Nano Lett.* **2007**, *7*, 2080.

AM900445E